COMMUNICATION

Check for updates

3D printing of reactive macroporous polymers *via* thiol–ene chemistry and polymerization-induced phase separation†‡

Nikolaj K. Mandsberg, §[a] Fatma Aslan, §[a] Zheqin Dong*[ab] and Pavel A. Levkin *[ac]

Using thiol–ene chemistry, polymerization-induced phase separation, and DLP 3D printing, we present a method for manufacturing reactive macroporous 3D structures. This approach enables the fabrication of structures with tunable physicochemical properties and compressibility. Moreover, it facilitates post-functionalization through thiol-Michael addition reactions, thereby expanding performance and application potential.

Macroporous polymers, featuring pore diameters of >50 nm, exhibit a unique combination of high surface area, rapid mass transport, and selective permeability,[1] making them suitable for applications as diverse as chromatography,[2] adsorptive water purification,[3] enzyme catalysis,[4] drug delivery,[5] air filtration,[6] mechanical and acoustic modulation,[7] and biomedical and tissue engineering.[8] The broad applicability of macroporous polymers hinges on their chemical functionality and 3D geometry.[9] To date, most of them are prepared through bulk polymerization or solution casting, with limited control over their macro-geometry.[10]

The integration of 3D printing technology in producing macroporous materials could further broaden their potential uses. Recent strides in this direction have been achieved through the introduction of polymerization-induced phase-separation to light-based 3D printing systems.[11–13] This approach enables *in situ* generation and control of macroporosity, while concurrently shaping the macro-geometry. The method has significantly increased the achievable geometrical complexity, already finding use in applications like miniaturized Ulbricht light-integrating spheres,[11] objects with superhydrophobicity,[13] and membranes.[14]

However, this existing research has primarily focused on (meth)acrylate photopolymerization and optimization of its porosity, with limited exploration of photoresist systems that mitigate brittleness – as a result, their mechanical fragility limits practical use. Thiol–ene-based polymerization, known for its simplicity, stands out as a potential solution.[15] Not only could it increase structural flexibility to improve mechanical stability, but it also allows for click-type post-modification, thereby deriving multiple functionalities from a single resin system.[16] These advantages make thiol–ene polymerization a promising avenue.

Here, we propose a method for 3D printing mechanically stable, reactive macroporous structures by combining thiol–ene chemistry with polymerization-induced phase separation and digital light projection (DLP) 3D printing. This method allows independent control of the physical structure and chemical functionality of 3D printed macroporous polymers. Our findings highlight the resin systems' flexibility in forming diverse geometries, reveal variations in both porosity and mechanical properties across resin types, as well as demonstrate the ability to create chemical surface patterns on 3D objects.

Thiol–ene chemistry was integrated with DLP 3D printing and polymerization-induced phase separation to create porous structures. Upon UV activation, the thiol and alkene components undergo a crosslinking reaction in the presence of porogens, leading to simultaneous phase separation as shown in Fig. 1A. The method includes washing with acetone to remove the unreacted liquid porogen phase, followed by critical point drying to maintain the surface porosity. This results in a polymer macrostructure with inherent porosity filled with air (see Fig. 1B). The resin composition (Fig. 1C) consists of a thiol component (pentaerythritol tetrakis(3-mercaptopropionate), PETMP) with four functional groups, and a

[a] Karlsruhe Institute of Technology (KIT), Institute of Biological and Chemical Systems – Functional Molecular Systems (IBCS-FMS), Kaiserstrasse 12, Karlsruhe 76131, Germany. E-mail: zheqindong@sdu.edu.cn, levkin@kit.edu

[b] School and Hospital of Stomatology Cheeloo College of Medicine Shandong University & Shandong Key Laboratory of Oral Tissue Regeneration & Shandong Engineering Laboratory for Dental Materials and Oral Tissue Regeneration No. 44-1 Wenhuaxi Road, Jinan, Shandong 250012, China

[c] Karlsruhe Institute of Technology (KIT), Institute of Organic Chemistry (IOC), Kaiserstrasse 12, Karlsruhe 76131, Germany

† Electronic supplementary information (ESI) available: Details for materials manufacturing, characterizations, and additional results. Figures include chemical patterning methodology, SEM analysis, pore size distributions, hydrophobicity characterization, raw Raman spectra, porogen screening by bulk polymerization, and material transmission spectra. See DOI: https://doi.org/10.1039/d4cc00466c

‡ Additional data available upon request or in RADAR4KIT repository: https://doi.org/10.35097/1978.

§ These authors contributed equally.

Fig. 1 DLP printing of thiol–ene based porous 3D structures. (A) DLP printing process using phase-separating thiol–ene resin. (B) Top: 3D printed object after supercritical drying; Bottom: Cross-sectional SEM showing porosity. (C) Structure of key resin ingredients: (1) pentaerythritol tetrakis(3-mercaptopropionate) (PETMP), (2) tri(ethyleneglycol)divinylether (TEG), (3) polyethylene glycol 200. (D) Various printed geometries showcasing resin versatility. (E) Reversible compression of the printed structure.

of our thiol–ene polymers exhibits a Young's modulus of 13 MPa, which is significantly lower than the 202 MPa observed in a methacrylate-based reference polymer.[12] This reduced stiffness contributes to greater elasticity (see Fig. 1E), which is an advantageous property for many practical applications where flexibility and mechanical stability are important.[17]

Mechanical compressibility of the macroporous polymers was tested using cyclic compressive loading-unloading stress–strain with increasing upper limit and constant lower limit (testing was along the printing direction with 10% min^{-1} loading/unloading rate) (Fig. 2A).[18] As reference, methacrylate-based macroporous polymers (50% porogen) were printed according to the literature[12] (see ESI†) and the thiol–ene-based resin prepared with 50 wt% of PEG and a thiol:alkene (PETMP:TEG) stoichiometric molar ratio of 1:2. We observed that these thiol–ene porous polymer cubes can bear a cyclic compressive strain higher than 50%, as opposed to $\sim$30% for the corresponding polymethacrylate cubes. Furthermore, they demonstrate good elastic recoverability as is evident by comparing the hysteresis loops, which is further quantified in Fig. 2B using the relative energy recovery (calculated as area under the unloading curve normalized with respect to area under the loading curve) for the different maximum strains. At 30% strain, the recovery was 80% for the thiol–ene-based porous structures, while mere 23% for the polymethacrylate ones.

We hypothesize that the enhanced elasticity is due to a multi-faceted interplay between the pronounced cross-linking of the thiol–ene polymer and the presence of PEG additives that play a plasticizing role to further enhance flexibility by reducing intermolecular forces.[19] Our findings are consistent with previous research where thiol–ene-based polymers typically exhibit a lower modulus compared to methacrylate-based polymers, despite the higher monomer conversion rate of the former.[20,21]

Different concentrations of PEG200 porogen (40 wt%, 50 wt%, and 70 wt%) were employed to modify the porosity of thiol–ene polymers. Scanning electron microscope images,

bifunctional alkene component (tri(ethyleneglycol)divinylether, TEG). The PETMP serves primarily as a crosslinking agent due to its higher functionality, while TEG acts in conjunction with PETMP to form the crosslinked network. Polyethylene glycol (PEG200) is used as a porogen because of its good miscibility with the reactive components but limited solubility in the cured matrix (see Table S2 and Fig. S6 for all tested porogens, ESI†). The resulting phase immiscibility during the polymerization process is crucial for developing the porous architecture. The photopolymerization process is catalysed by Irgacure 819, with Sudan I dye as a light-absorbing agent to enhance vertical resolution and the (2,2,6,6-tetramethylpiperidin-1-yl)oxyl (TEMPO) radical scavenger fine-tuning the lateral resolution to match the mirror array unit cell size of the DLP system. The resin system is compatible with various 3D structures, ranging from basic cubes to complex geometries with overhangs, hierarchical porosity, and chirality (see Fig. 1D). See ESI† for more detailed manufacturing protocol.

Our research reveals that the thiol–ene based polymers exhibit significantly lower stiffness than traditional methacrylate-based polymers used in 3D printing. Specifically, the non-porous version

Fig. 2 Comparative cyclic compressibility and energy recovery. (A) Cyclic compressibility of a porous thiol–ene and methacrylate-based material. (B) Energy recovery calculated for both materials using the ratio between the areas under the unloading and loading curves.
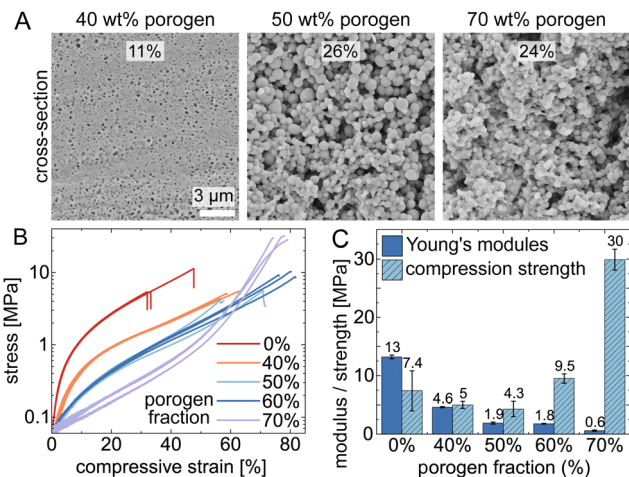
Fig. 3 Impact of porogen weight fraction on the porous structure. (A) SEM images cross-sections of selected 5 mm 3D-printed cubes. Porosity is calculated using adaptive thresholding. (B) Stress–strain curves. (C) Calculated Young's moduli and compression strengths.

as shown in Fig. 3A, illustrate this porosity on cross-sections of the printed cubes (see Fig. S3 for pore size distributions showing mean pore diameters >100 nm, ESI†). Samples with higher porogen content also exhibited a marked increase in volumetric shrinkage, increasing from 7.75% to 60.4%. This change is attributed to increased porosity due to higher fraction of porogen, highlighting the significant influence of porogen on the material's properties. As porosity increases, we could expect an enhancement in the structures' elasticity. Indeed, objects printed without porogen were notably fragile exhibiting a maximum compressive strain of approximately 30%, whereas those created with porogen solvent, facilitating phase separation, yielded significantly more elastic, soft materials with maximum compressive strain higher than 50%.

As a result, we explore how varying levels of porosity affect the mechanical properties of cube-shaped thiol–ene-based polymers. Fig. 3B illustrates stress–strain curves and compression test data (along the print direction), showing that different porogen fractions (0, 40, 50, 60, 70 wt%) combined with a constant cross-linker stoichiometric molar ratio (thiol : alkene; 1 : 2) result in diverse mechanical properties. As shown in Fig. 3C, the Young's modulus (E) decreases significantly with increasing porogen content, while the compression strength (σ) does not change significantly until >50% porogen, where it eventually increases. Respectively, their values change from 13 MPa and 7.4 MPa in porogen-free samples (0 wt%) to 0.6 MPa and 30 MPa in samples with 70 wt% PEG200, demonstrating that the porogen fraction substantially influences the material's mechanical properties. We hypothesize that the observed increase in compressive strength may be attributed to changes in pore geometry rather than porosity.[22] Evidently, the macroporosity can markedly alter the mechanical resilience of 3D-printed polymeric materials. For comparison, an 80% porous non-3D printed macroporous PMMA has $E \sim 85$ MPa and $\sigma \sim 5$ MPa.[23]

An advantage of thiol–ene based polymerization is the ability to access free thiol groups (or double bonds) through off-stoichiometry. This enables additional chemical functionalization

through thiol–ene Michael or radical reactions. To illustrate this potential, we initially showcased the bulk functionalization of 3D printed macroporous polymer structures using Michael-type thiol–ene conjugation.[24] In this case, objects prepared with off-stoichiometry thiol–ene (OSTE) formulations were subjected to thiol-Michael addition reactions using two different acrylates: 1*H*,1*H*,2*H*,2*H*-perfluorodecyl acrylate (PFDA, hydrophobic) and 2-hydroxyethyl methacrylate (HEMA, hydrophilic), which effectively altered the wettability properties of the materials.

The wettability of $5 \times 5 \times 5$ mm³ thiol–ene cubes printed with OSTE molar ratios of 1.50 : 2.0 (PETMP : TEG) underwent significant changes due to the modifications. Initially, the unmodified material exhibited moderate hydrophilicity with a maximum/initial apparent contact angle (CA) of 62°, as shown in Fig. 4A. After modification, Fig. 4B shows a marked increase in hydrophobicity, with the CA increasing to 135° for the surface and 155° for the cross section, confirming the effectiveness of the reaction throughout the 3D printed object, supporting its potential for applications that require robust superhydrophobicity.[25] Interestingly, the CA for the bulk material is slightly higher than that of the surface. This difference can be attributed to the rougher structure of the cross-section in comparison to the surface (see ESI†). On the other hand, for HEMA, the focus was on increasing hydrophilicity to improve water wicking, as shown in Fig. 4C. This enhancement is quantified in Fig. 4D, which compares the wicking behaviour on both the surface and a cross section of the modified material, showing a reduced maximum/initial CA and different wicking rates. The success of these functionalizations in enhancing both hydrophobic and hydrophilic properties was further confirmed by Raman spectroscopy of the surfaces. Fig. 4E demonstrates this by showing a decrease in the intensity of the S–H stretching band at ~ 2575 cm^{-1} in the modified structures.

Finally, we demonstrated the possibility of selective functionalization of 3D-printed macroporous structures *via* thiol–ene radical reaction (Fig. 4F). Such an ability to chemically pattern the surface of three-dimensional objects is important for the combined shaping and chemical functionalization of 3D structures.[26] Our resin system facilitates such patterning, as exemplified in a two-step functionalization process using a 3D photomask (details in Fig. S1, ESI†): First, a localized click reaction was used to render subregions hydrophilic, which effectively consumed the thiols in those areas. This was followed by the hydrophobization of the remaining exposed thiols, modifying both the overall bulk and the unreacted surface areas of the material. The modified structure consists of 2 mm hydrophilic patches within a hydrophobic matrix, showcasing selective water attraction and repulsion in one object. For visual evidence, see the ESI† video.

In summary, a method for 3D printing thiol–ene macroporous polymers *via* polymerization-induced phase separation was developed, exploring the interplay between ink formulation, pore structure, and mechanical properties. Comparative analyses revealed that thiol–ene based networks possess enhanced elasticity compared to polymethacrylates, characterized by a 50% reversible compressibility. The introduction of off-stoichiometry enables both surface and bulk functionalization of these materials, including
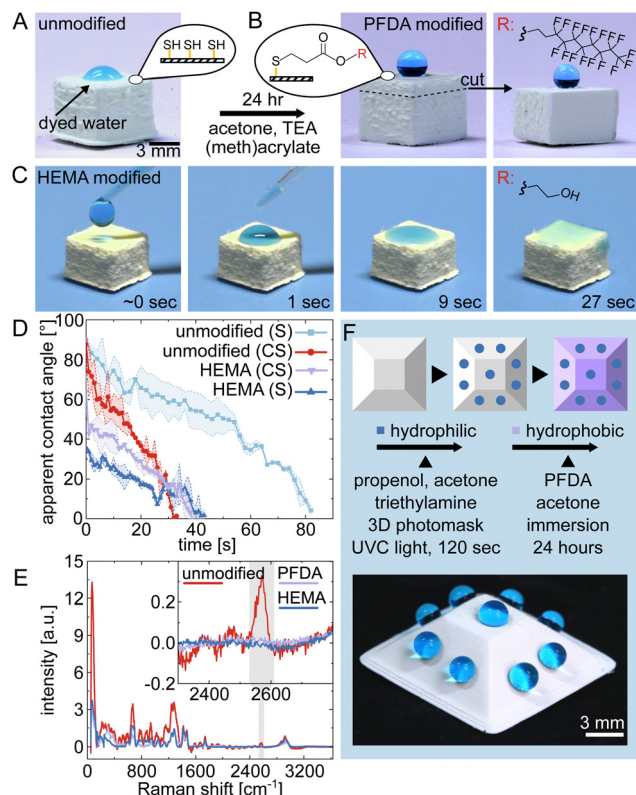
Fig. 4 Post-modification effects on thiol–ene porous polymer cubes. Photos illustrating the different wettability of (A) as-printed material, (B) hydrophobically (PFDA) and (C) hydrophilically (HEMA) functionalized. (D) Wicking dynamics of unmodified *vs.* HEMA-modified cubes; S = surface and CS = cross-section. (E) Raman spectra comparing surfaces of unmodified and modified cubes. (F) Bifunctional chemical wettability patterning on a 3D object with adherent water droplets.

chemical patterning, as evidenced by changes in wetting properties, verified by water contact angle and Raman spectroscopy.

The method presented here contributes to the evolving landscape of 3D-sculpted macroporous polymers, particularly in tailoring their mechanical properties and enabling chemical patterning with (photo-initiated) click-chemistry. Wettability patterning is just one example of chemical patterning, but finds applications in fog harvesting,[27] anti-counterfeit,[28] spatial control of nucleation[29] for crystal growth,[30] and programmable cell migration[31] – these studies were based on monotonic chemical gradients or 2D patterns. Chemical patterning of 3D objects multiplies the possibilities, highlighting its potential as a versatile tool in the field of 3D printed macroporous materials.

N. K. M: formal analysis, funding acquisition, investigation, methodology, visualization, writing – original draft, writing – review editing. F. A.: formal analysis, investigation, visualization, writing – original draft. Z. D.: conceptualization, methodology, supervision, visualization, writing – review editing. P. A. L.: conceptualization, funding acquisition, methodology, supervision, writing – review editing.

Conflicts of interest

There are no conflicts to declare.

Notes and references

1 F. Svec and J. M. J. Fréchet, *Science*, 1996, **273**, 205–211.
2 R. D. Arrua, M. Talebi, T. J. Causon and E. F. Hilder, *Anal. Chim. Acta*, 2012, **738**, 1–12.
3 B. Wang, P. Prinsen, H. Wang, Z. Bai, H. Wang, R. Luque and J. Xuan, *Chem. Soc. Rev.*, 2017, **46**, 855–914.
4 P. Lozano, E. García-Verdugo, R. Piamtongkam, N. Karbass, T. De Diego, M. I. Burguete, S. V. Luis and J. L. Iborra, *Adv. Synth. Catal.*, 2007, **349**, 1077–1084.
5 C. Canal, R. M. Aparicio, A. Vilchez, J. Esquena and M. J. García-Celma, *J. Pharm. Pharm. Sci.*, 2012, **15**, 197.
6 S. J. Kim and S. C. Jana, *Polymer*, 2017, **126**, 432–436.
7 A. Kovalenko, T. Brunet and O. Mondain-Monval, *Polymer*, 2018, **148**, 239–246.
8 M. Pagac, J. Hajnys, Q.-P. Ma, L. Jancar, J. Jansa, P. Stefek and J. Mesicek, *Polymers*, 2021, **13**, 598.
9 R. D. Arrua, M. C. Strumia and C. I. Alvarez Igarzabal, *Materials*, 2009, **2**, 2429–2466.
10 D. Wu, F. Xu, B. Sun, R. Fu, H. He and K. Matyjaszewski, *Chem. Rev.*, 2012, **112**, 3959–4015.
11 F. Mayer, D. Ryklin, I. Wacker, R. Curticean, M. Čalkovský, A. Niemeyer, Z. Dong, P. A. Levkin, D. Gerthsen, R. R. Schröder and M. Wegener, *Adv. Mater.*, 2020, **32**, 2002044.
12 Z. Dong, H. Cui, H. Zhang, F. Wang, X. Zhan, F. Mayer, B. Nestler, M. Wegener and P. A. Levkin, *Nat. Commun.*, 2021, **12**, 247.
13 Z. Dong, M. Vuckovac, W. Cui, Q. Zhou, R. H. A. Ras and P. A. Levkin, *Adv. Mater.*, 2021, **33**, 2106068.
14 F. Mayoussi, E. H. Doeven, A. Kick, A. Goralczyk, Y. Thomann, P. Risch, R. M. Guijt, F. Kotz, D. Helmer and B. E. Rapp, *J. Mater. Chem. A*, 2021, **9**, 21379–21386.
15 Z. Liu, J. Ou, H. Lin, Z. Liu, H. Wang, J. Dong and H. Zou, *Chem. Commun.*, 2014, **50**, 9288–9290.
16 C. E. Hoyle and C. N. Bowman, *Angew. Chem., Int. Ed.*, 2010, 49, 1540–1573.
17 G. Wang, T. Zhao, L. Chen, K. Liu, R. Fang and M. Liu, *Langmuir*, 2020, **36**, 10794–10802.
18 C. Han, D. Li, Y. Rao and J. Wang, *IOP Conf. Ser. Earth Environ. Sci.*, 2020, **570**, 032024.
19 Z. Wang, H. Cui, M. Liu, S. L. Grage, M. Hoffmann, E. Sedghamiz, W. Wenzel and P. A. Levkin, *Adv. Mater.*, 2022, **34**, 2107791.
20 H. Lu, J. A. Carioscia, J. W. Stansbury and C. N. Bowman, *Dent. Mater.*, 2005, **21**, 1129–1136.
21 S. M. Trey, E. Kristofer Gamstedt, E. Mäder, S. Jönsson and M. Johansson, *Composites, Part A*, 2011, **42**, 1800–1808.
22 L. Griffiths, M. J. Heap, T. Xu, C. Chen and P. Baud, *J. Struct. Geol.*, 2017, **96**, 149–160.
23 K. M. Althubeiti and T. S. Horozov, *React. Funct. Polym.*, 2019, **142**, 207–212.
24 D. P. Nair, M. Podgórski, S. Chatani, T. Gong, W. Xi, C. R. Fenoli and C. N. Bowman, *Chem. Mater.*, 2014, **26**, 724–744.
25 D. Wang, Q. Sun, M. J. Hokkanen, C. Zhang, F. Y. Lin, Q. Liu, S. P. Zhu, T. Zhou, Q. Chang, B. He, Q. Zhou, L. Chen, Z. Wang, R. H. A. Ras and X. Deng, *Nature*, 2020, **582**, 55–59.
26 Z. Dong, J. Monti, H. Cui, A. Welle, S. A. Singaraju, E. Blasco and P. A. Levkin, *Adv. Mater. Technol.*, 2023, **8**, 2201268.
27 J. Ju, K. Xiao, X. Yao, H. Bai and L. Jiang, *Adv. Mater.*, 2013, **25**, 5937–5942.
28 I. B. Burgess, L. Mishchenko, B. D. Hatton, M. Kolle, M. Lončar and J. Aizenberg, *J. Am. Chem. Soc.*, 2011, **133**, 12430–12432.
29 N. K. Mandsberg, *Adv. Mater. Interfaces*, 2021, **8**, 1–16.
30 J. Aizenberg, A. J. Black and G. M. Whitesides, *Nature*, 1999, **398**, 495–498.
31 J. H. Lee, G. Khang, J. W. Lee and H. B. Lee, *J. Colloid Interface Sci.*, 1998, **205**, 323–330.